

1 **Wave dispersion in a damped beam supported by cubic nonlinear springs: A**
2 **multiscale freewave approach**

3 Abhigna Bhatt*

4 *Department of Civil Engineering, Indian Institute of Technology Delhi, India*

5 Kamal K. Bera†

6 *Department of Civil Engineering, National Institute of Technology Tiruchirappalli, Tiruchirappalli, India*

7 Arnab Banerjee‡

8 *Department of Civil Engineering, Indian Institute of Technology Delhi, India*

9 (Dated: May 6, 2025)

10 Researchers are drawn to exploring wave dispersion in nonlinear systems because of the amplitude-
11 dependent tunability of the bandgap. This paper investigates the amplitude-dependent wave dis-
12 persions in continuous beam structures supported periodically by nonlinear springs. Additionally, it
13 examines the influence of inherent beam damping on wave dispersion. The analytical framework
14 consists of homogenization of the unit cell and the method of multiple scales with two distinct
15 time scales to derive the wave dispersion equation. The proposed analytical approach for non-
16 linear wave propagation is validated through numerical finite element simulations. It is observed
17 that the frequency shift is positive for hardening and negative for softening supports. Following
18 this, the dispersion shift over time in the damped systems is examined by considering viscous and
19 strain rate-dependent damping. The sensitivity of strain rate damping to propagation constant and
20 the independence of viscous damping from propagation constant are thoroughly investigated. In a
21 damped system, the frequency shift diminishes over time as the amplitude decreases reducing the
22 effect of nonlinearity. This study opens up avenues for controlling or filtering vibrations through
23 the tunable bandgap of continuous nonlinear metamaterials.

24 **Keywords:** Homogenisation, Method of multiple scales, Frequency shift, Amplitude modulation, Amplitude
25 dependant dispersion

26 **I. INTRODUCTION**

27 Over the past decade, wave dispersion in linear meta-
28 materials has garnered considerable attention from re-
29 searchers due to its complex dispersion patterns, filtering
30 capabilities, and the emergence of frequency bandgaps.
31 The presence of nonlinearities within these systems has
32 further piqued the interest of the engineering commu-
33 nity, revealing fascinating phenomena such as amplitude-
34 dependent dispersion and alterations in group velocity
35 with weak nonlinear effects, as well as the propagation of
36 solitary waves like solitons under strong nonlinear condi-
37 tions. This exploration of wave propagation in nonlinear
38 metamaterial has led to the proposal of various engineer-
39 ing applications, including diodes [1, 2], switches [3], and
40 filters [4].

41 Several recent studies have analyzed amplitude-
42 dependent dispersion in discrete nondispersive systems
43 such as monoatomic and diatomic chains with cubic non-
44 linearity using perturbation method [5], nonlinear tri-
45 atomic metamaterial [6, 7], monoatomic chain with non-
46 linear embedded resonator [8], nonlinear monoatomic
47 chain with embedded resonator[9, 42], nonlinear ro-

48 ton like chain[11] etc. Additionally, nonlinear be-
49 havior such as amplitude-induced bandgap[10, 12], self-
50 switching functionality [13], bridging coupling mecha-
51 nism [14], band tunability [43] and nonreciprocity [44, 45]
52 etc has been observed in variety of discrete systems.
53 Different analytical methods such as Lindstedt–Poincaré
54 perturbation technique, method of multiscale, harmonic
55 balance method, method of averaging, Jacobi’s elliptic
56 balance method [60] etc [15, 16] have been used in deriv-
57 ing analytical solutions of the nonlinear dynamic systems
58 in the past. However, the method of multiple scales is
59 well suited for the damped system as it solves for ampli-
60 tude modulation [17–20]. In the case of nonlinear contin-
61 uous systems, researchers generally tackle finite systems
62 and obtain frequency response function [21–28]. In non-
63 linear continuum elastic media with topological mechan-
64 ics the method of multiple scales is widely used [58, 59].
65 In the case of continuous infinite structures, the nonlin-
66 ear dispersion shift is obtained for a few systems such
67 as a bar with periodically embedded resonators [29–31],
68 beam with periodic resonators [32, 33] etc. The quasi-
69 static wide bandgap can be induced by a beam on an
70 elastic foundation for linear systems [35]. Additionally
71 by incorporating nonlinear supports, the tunable quasi-
72 static bandgap can be obtained [36]. This has motivat-
73 ed us to study the amplitude-dependent wave dispersion in
74 infinite long periodically supported damped beams.

* Abhigna.Sandipkumar.Bhatt@civil.iitd.ac.in

† kamal@nitt.edu

‡ abanerjee@iitd.ac.in

75 An infinite beam with damping and nonlinear sup-
76 ports has numerous practical applications. For instance,

railway tracks can be modeled as infinitely long Euler-Bernoulli beams resting on nonlinear spring-dashpot systems, making the study of flexural wave propagation essential for the analysis, design, and health monitoring of railway infrastructure [46–48]. Additionally, functionally graded foams, which can be modeled as beams supported by nonlinear springs with damping [55], are widely used in various fields. These include acoustic control [53], shock and energy absorption [49, 50], as well as applications in the automotive industry [51] and biomedical instruments [52]. Furthermore, beams on periodic elastic foundations are key for achieving wider bandgap regions and stronger attenuation capabilities [56], enhancing passive vibration control [54] and other advanced engineering solutions.

Historically, researchers have directed their attention towards both nonlinear and linear wave propagation within discrete metamaterials, while investigations into wave propagation in continuous metamaterials have primarily focused on linear systems. Concerning nonlinear continuous systems, researchers have primarily explored frequency response functions within various finite systems, leaving a limited examination of wave propagation within continuous beam systems incorporating nonlinearity [34].

To address this gap, the study delves into the amplitude-dependent, time-varying dispersion relation of a damped beam supported by nonlinear springs. Specifically, it explores the wave dispersion relation of a damped beam supported by periodic nonlinear structures, considering two types of damping—viscous and strain rate damping—alongside both softening and hardening cubic nonlinearity. Employing a multiscale method with two distinct time scales, the study analytically derives the wave dispersion equation. The accuracy of the analytical solution is confirmed through comparison with numerical results. Initially, the paper discusses the frequency shift in undamped systems affected by hardening and softening nonlinearities. Subsequently, it examines the dispersion shift over time in damped systems, distinguishing between viscous and strain rate damping. The sensitivity of strain rate damping to propagation constants and the independence of viscous damping from propagation constants are thoroughly investigated. In summary, the paper extensively explores the amplitude-dependent nonlinear dispersion in infinitely long damped beams periodically supported by nonlinear springs. These are vital for modeling railway tracks, functionally graded foams, and enhancing passive vibration control in various engineering applications.

II. METHODOLOGY

Considering the flexural wave propagation in infinitely long Euler Bernoulli beam supported by cubic nonlinear springs as depicted in Fig. 1(a), the following analytical formulation is derived.

A. Governing equation

The governing equation of motion of the representative unit cell shown in Fig. 1(b) can be written as [37]:

$$\frac{\partial^2}{\partial x^2} \left(EI \frac{\partial^2 w}{\partial x^2} + C_s \frac{\partial^3 w}{\partial x^2 \partial t} \right) + \rho A \frac{\partial^2 w}{\partial t^2} + C_a \frac{\partial w}{\partial t} + \left(\tilde{k}_1 w + \tilde{k}_3 w^3 \right) \delta(x) = 0 \quad (1)$$

where, EI = flexural rigidity, C_s = strain rate-dependent damping, C_a = velocity-dependent viscous damping, ρ = density, A = cross-section area, \tilde{k}_1 and \tilde{k}_3 are liner and nonlinear spring stiffness, w denotes transverse deflection, x = distance, and t represents time. Further, the Dirac delta function was approximated using a homogenization approach in which the stiffness of the spring was scaled down by the inverse of the length of the unit cell ($1/l$) as [38].

$$\frac{\partial^2}{\partial x^2} \left(EI \frac{\partial^2 w}{\partial x^2} + C_s \frac{\partial^3 w}{\partial x^2 \partial t} \right) + \rho A \frac{\partial^2 w}{\partial t^2} + C_a \frac{\partial w}{\partial t} + \frac{1}{l} \left(\tilde{k}_1 w + \tilde{k}_3 w^3 \right) = 0 \quad (2)$$

Further, the governing equation can be written as

$$\frac{\partial^2 w}{\partial t^2} + \omega_n^2 \frac{\partial^4 w}{\partial x^4} + k_1 w + c_1 \frac{\partial w}{\partial t} + c_2 \frac{\partial^5 w}{\partial x^4 \partial t} + k_3 w^3 = 0 \quad (3)$$

where, $\omega_n^2 = \frac{EI}{\rho A}$, $c_1 = \frac{C_s}{\rho A}$, $c_2 = \frac{C_a}{\rho A l}$, $k_1 = \frac{1}{\rho A l} \tilde{k}_1$ and $k_3 = \frac{1}{\rho A l} \tilde{k}_3$

B. Multiple scales Method

The nonlinear governing equation given in Eq. (3) has been solved using the method of multiple scales by introducing the scaling parameter ϵ with damping and nonlinear terms as:

$$\frac{\partial^2 w}{\partial t^2} + \omega_n^2 \frac{\partial^4 w}{\partial x^4} + k_1 w + \epsilon \left(c_1 \frac{\partial w}{\partial t} + c_2 \frac{\partial^5 w}{\partial x^4 \partial t} + k_3 w^3 \right) = 0 \quad (4)$$

The nonlinear partial differential equation, as presented in Eq. (4), involves independent variables x and t corresponding to spatial and temporal dimensions, respectively. The method of multiple scales can be applied by employing slow time scales or large space scales. Here, by employing a multiscale approach, additional scales are introduced to account for slow time scale, denoted as $T_1 = \epsilon t$. These augment the original scales for time $T_0 = t$. Another way of the multiple scales method by employing spatial expansion is demonstrated in Appendix A. The time derivatives can be written as

$$\frac{\partial}{\partial t} = \frac{\partial}{\partial T_0} + \epsilon \frac{\partial}{\partial T_1} \quad (5)$$

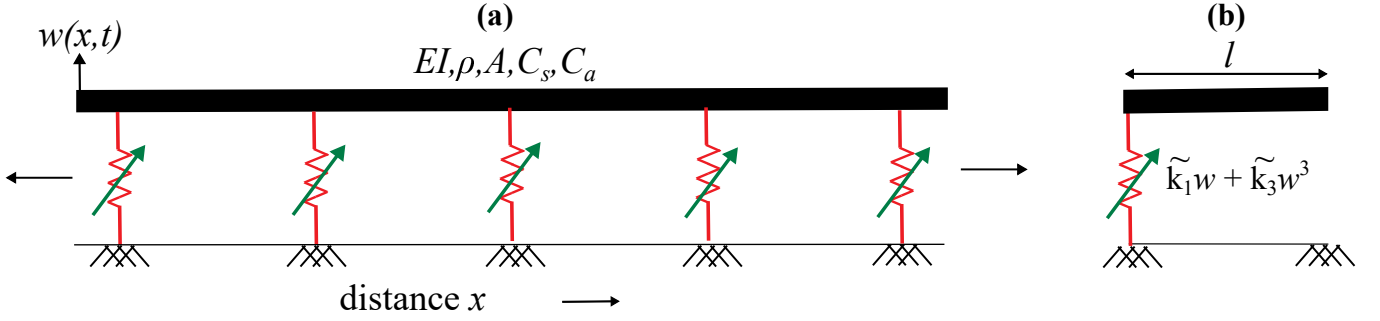


FIG. 1. (a) The Euler Bernoulli beam periodically supported by nonlinear springs (b) The representative unit cell

171 Further, the solution can be obtained as

$$172 \quad w(x, t, \epsilon) = \sum_{n=0}^1 \epsilon^n w_n(x, T_0, T_1) + O(\epsilon) \quad (6)$$

173 By substituting the solution given in Eq. (6) into the
174 partial differential equation (Eq. (4)) and employing the
175 temporal derivatives provided in Eq. (5), yields

$$\begin{aligned} 176 \quad & \epsilon^2 \left(\frac{\partial^2 w_0}{\partial T_1^2} + 2 \frac{\partial^2 w_1}{\partial T_1 \partial T_0} \right) + \epsilon^3 \frac{\partial^2 w_1}{\partial T_1^2} \\ 177 \quad & + \epsilon \left(2 \frac{\partial^2 w_0}{\partial T_1 \partial T_0} + \frac{\partial^2 w_1}{\partial T_0^2} \right) + \frac{\partial^2 w_0}{\partial T_0^2} + \omega_n^2 \left(\epsilon \frac{\partial^4 w_1}{\partial x^4} + \frac{\partial^4 w_0}{\partial x^4} \right) \\ 178 \quad & + k_1 (w_0 + \epsilon w_1) + c_1 \epsilon \left(\frac{\partial w_0}{\partial T_0} + \epsilon^2 \frac{\partial w_1}{\partial T_1} + \epsilon \left(\frac{\partial w_1}{\partial T_0} + \frac{\partial w_0}{\partial T_1} \right) \right) \\ 179 \quad & + c_2 \epsilon \left(\epsilon^2 \frac{\partial^5 w_1}{\partial x^4 \partial T_1} + \epsilon \left(\frac{\partial^5 w_1}{\partial x^4 \partial T_0} + \frac{\partial^5 w_0}{\partial x^4 \partial T_1} \right) + \frac{\partial^5 w_0}{\partial x^4 \partial T_0} \right) \\ 180 \quad & + \epsilon k_3 (w_0 + \epsilon w_1)^3 = 0 \end{aligned} \quad (7)$$

181 Further, collecting terms with a similar power of ϵ , the
182 following equation can be written.

$$\begin{aligned} 183 \quad & \frac{\partial^2 w_0}{\partial T_0^2} + \frac{\partial^4 w_0}{\partial x^4} + k_1 w_0 \\ 184 \quad & + \epsilon \left(\frac{\partial^2 w_1}{\partial T_0^2} + 2 \frac{\partial^2 w_0}{\partial T_1 \partial T_0} + \frac{\partial^4 w_1}{\partial x^4} + k_1 w_1 \right) \\ 185 \quad & + \epsilon \left(c_1 \frac{\partial w_0}{\partial T_0} + c_2 \frac{\partial^5 w_0}{\partial x^4 \partial T_0} + k_3 w_0^3 \right) + O(\epsilon^2) = 0 \end{aligned} \quad (8)$$

186 The governing partial differential equations can be ex-
187 pressed through the consolidation of terms with similar
188 powers of ϵ as.

$$189 \quad R_0 + R_1 \epsilon + O(\epsilon^2) = 0 \quad (9)$$

190 where

$$191 \quad R_0 : \frac{\partial^2 w_0}{\partial T_0^2} + \frac{\partial^4 w_0}{\partial x^4} + k_1 w_0 = 0 \quad (10)$$

$$\begin{aligned} 192 \quad R_1 : & \frac{\partial^2 w_1}{\partial T_0^2} + 2 \frac{\partial^2 w_0}{\partial T_1 \partial T_0} + \frac{\partial^4 w_1}{\partial x^4} + k_1 w_1 \\ 193 \quad & + c_1 \frac{\partial w_0}{\partial T_0} + c_2 \frac{\partial^5 w_0}{\partial x^4 \partial T_0} + k_3 w_0^3 = 0 \end{aligned} \quad (11)$$

194 Eq. (9) expands the nonlinear equation of motion in
195 orders of (ϵ) , matching it to the zeroth order and first
196 order in (ϵ) . The solutions w_0 , and w_1 can be obtained
197 by solving equations $R_0 = 0$ and $R_1 = 0$ in progression.

198 In the case of flexural wave solution in infinite structure,
199 the boundary complexities can be ignored and the
200 plane wave solution can be assumed for the equation
201 $R_0 = 0$ as [39].

$$202 \quad w_0 = A(T_1) e^{i(\kappa x - \omega T_0)} + \bar{A}(T_1) e^{-i(\kappa x - \omega T_0)} \quad (12)$$

203 Substituting Eq. (12) in Eq. (10) the dispersion relation
204 for the linear system can be derived as

$$205 \quad \kappa^4 - \omega^2 + k_1 = 0 \quad (13)$$

206 Further, substituting Eq. (12) in Eq. (11), the following
207 equation can be obtained

$$\begin{aligned} 208 \quad & \frac{\partial^2 w_1}{\partial T_0^2} + \frac{\partial^4 w_1}{\partial x^4} + k_1 w_1 \\ 209 \quad & = \left(2i\omega \frac{\partial A}{\partial T_1} + ic_1 \omega A + ic_2 \kappa^4 \omega A - 3k_3 A^2 \bar{A} \right) e^{i(\kappa x - \omega T_0)} \\ 210 \quad & - k_3 A^3 e^{i(3\kappa x - 3\omega T_0)} + cc \end{aligned} \quad (14)$$

211 The particular solution of Eq. (14) contains secular terms
212 which lead to nonuniform expansion in scaled time. Since
213 the linear operator $\left(\frac{\partial^2}{\partial T_0^2} + \frac{\partial^4}{\partial x^4} + k_1 \right)$ is self-adjoint, as
214 demonstrated in the Appendix B, the solvability condition
215 for eliminating secular terms can be derived. This
216 condition is obtained by equating the forcing terms re-
217 sponsible for generating the secular terms to zero, which
218 leads to the following partial differential equation gov-
219 erning the amplitude A .

$$220 \quad 2i\omega \frac{\partial A}{\partial T_1} + ic_1 \omega A + ic_2 \kappa^4 \omega A - 3k_3 A^2 \bar{A} = 0$$

$$221 \quad i \frac{\partial A}{\partial T_1} = -iA \left(\frac{c_1 + c_2 \kappa^4}{2} \right) + \frac{3}{2} k_3 \omega^{-1} A^2 \bar{A} \quad (15)$$

222 The solution of amplitude A in polar form can be as-
223 sumed as $A = \frac{1}{2}a(T_1)e^{i\beta(T_1)}$ and its complex conjugate,
224 $\bar{A} = \frac{1}{2}a(T_1)e^{-i\beta(T_1)}$. Further, the frequency shift due to

nonlinearity will be later demonstrated and reflected by²⁵⁸
the complex-valued phase of amplitude modulation. As
the phase β is a function of slow time scale (T_1) it essen-²⁵⁹
tially captures the frequency shift due to nonlinearity.
To determine the phase, by substituting the amplitude
 A and \bar{A} into Eq. (15) the following equations can be²⁶⁰
obtained.

$$\begin{aligned} & i \frac{1}{2} \left(e^{i\beta} \frac{\partial a}{\partial T_1} + i e^{i\beta} a \frac{\partial \beta}{\partial T_1} \right) \\ & = -i \left(\frac{c_1 + c_2 \kappa^4}{2} \right) \frac{a}{2} e^{i\beta} + \frac{3}{2} k_3 \omega^{-1} e^{i\beta} \frac{a^3}{8} \end{aligned} \quad (16)$$

Further separating the real and imaginary parts following²⁶⁸
equations can be obtained.

$$\frac{\partial a}{\partial T_1} = - \left(\frac{c_1 + c_2 \kappa^4}{2} \right) a \quad (17)$$

$$\frac{\partial \beta}{\partial T_1} = - \frac{3}{8} k_3 \omega^{-1} a^2 \quad (18)$$

The amplitude modulation can be obtained by solving²⁷³
Eq. (17) as

$$a = a_0 e^{-\left(\frac{c_1+c_2\kappa^4}{2}\right)T_1} \quad (19)$$

Further, the frequency shift can be obtained by substi-²⁷⁷
tuting Eq. (19) into Eq. (18) as follows.

$$\begin{aligned} \frac{\partial \beta}{\partial T_1} & = -\frac{3}{8} k_3 \omega^{-1} a_0^2 e^{-(c_1+c_2\kappa^4)T_1} \\ \beta & = \frac{3}{8} \frac{k_3 \omega^{-1} a_0^2}{(c_1 + c_2 \kappa^4)} e^{-(c_1+c_2\kappa^4)T_1} + \beta_0 \end{aligned} \quad (20)$$

Further, the initial condition has been assumed as at²⁸²
 $T_1 = 0, \beta = 0$ and so, $\beta_0 = -\frac{3}{8} \frac{k_3 \omega^{-1} a_0^2}{(c_1 + c_2 \kappa^4)}$. The shift in²⁸³
frequency can be determined as

$$\begin{aligned} \beta & = \frac{3}{8} \frac{k_3 \omega^{-1} a_0^2}{(c_1 + c_2 \kappa^4)} e^{-(c_1+c_2\kappa^4)T_1} - \frac{3}{8} \frac{k_3 \omega^{-1} a_0^2}{(c_1 + c_2 \kappa^4)} \\ \beta & = -\frac{3}{8} \frac{k_3 \omega^{-1} a_0^2}{(c_1 + c_2 \kappa^4)} \left(1 - e^{-(c_1+c_2\kappa^4)T_1} \right) \end{aligned} \quad (21)$$

The wave solution can be written by substituting ampli-²⁸⁸
tude Eq. (19) and frequency shift Eq. (21) into Eq. (12)²⁸⁹
as

$$\begin{aligned} w_0 & = \frac{a_0}{2} e^{-\left(\frac{c_1+c_2\kappa^4}{2}\right)T_1} \\ & e^{-i\frac{3}{8} \frac{k_3 \omega^{-1} a_0^2}{(c_1 + c_2 \kappa^4)T_1} \left(1 - e^{-(c_1+c_2\kappa^4)T_1} \right) T_1} e^{i(\kappa x - \omega T_0)} + cc \end{aligned} \quad (22)$$

Further, substituting $T_0 = t$ and $T_1 = \epsilon t$,

$$\begin{aligned} w_0 & = \frac{a_0}{2} e^{-\left(\frac{c_1+c_2\kappa^4}{2}\right)\epsilon t} \\ & e^{-i\frac{3}{8} \frac{k_3 \omega^{-1} a_0^2}{(c_1 + c_2 \kappa^4)t} \left(1 - e^{-(c_1+c_2\kappa^4)\epsilon t} \right) t} e^{i(\kappa x - \omega t)} + cc \end{aligned} \quad (23)$$

The frequency shift can be written as

$$\omega_s = \omega + \frac{3}{8} \frac{k_3 \omega^{-1} a_0^2}{(c_1 + c_2 \kappa^4) t} \left(1 - e^{-(c_1+c_2\kappa^4)\epsilon t} \right) \quad (24)$$

To further clarify the frequency shift derived in Eq. (24), it is important to highlight that the system's nonlinearity leads to an amplitude-dependent frequency shift. Initially, when t is small and the amplitude is large, the nonlinearity induces a substantial frequency shift. As time progresses and damping reduces the amplitude, the corresponding frequency shift diminishes. This behavior illustrates the direct correlation between the wave amplitude and the magnitude of the frequency shift in nonlinear systems. However, in the case of an undamped system, substituting $c_1 = c_2 = 0$ in Eq. (15) following frequency shift and wave solution can be obtained.

$$\omega_s = \omega + \frac{3k_3 a_0^2}{8\omega} \epsilon \quad (25)$$

$$w_0 = a_0 e^{-\left(\frac{3k_3 a_0^2}{8\omega}\right)\epsilon t} e^{i(\kappa x - \omega t)} + cc \quad (26)$$

The amplitude-dependant dispersion relation of an undamped beam supported by nonlinear springs can be obtained by squaring Eq. (25), substituting $\kappa^4 + k_1$ at ω^2 and neglecting terms of ϵ^2 as

$$\omega_s^2 = \kappa^4 + k_1 + \epsilon \frac{3k_3 a_0^2}{4} \quad (27)$$

Note that, the strength of cubic nonlinearity is generally considered by factor $\Pi = \frac{\epsilon k_3 a_0^2}{k_1}$. The method of multiple scales is applicable in the conservative bounds as $|\Pi| < 0.1$ [41]. Moreover, when the system is damped, the amplitude is always decreasing and is independent of the strength of cubic nonlinearity as time progresses which makes the system always stable [19].

C. Finite element modelling

A finite element formulation of the Euler-Bernoulli beam on nonlinear elastic springs has been developed for numerical validation. A governing strong form equation for a representative unit cell is derived as Eq. (4). Let, $w(x, t) = \psi(x)q(t)$, where, $q(t) = \{u_i, u'_i, u_j, u'_j\}^T$; u_i and u'_i are displacement and slope at i^{th} node at time t . Further $\psi(x)$ is shape function defined by Hermite polynomial as $\psi(x) = [\psi_1 \ \psi_2 \ \psi_3 \ \psi_4]$ where,

$$\begin{aligned} \psi_1(x) & = \frac{1}{l^3} (2x^3 - 3x^2l + l^3) \\ \psi_2(x) & = \frac{1}{l^3} (x^3l - 2x^2l^2 + xl^3) \\ \psi_3(x) & = \frac{1}{l^3} (-2x^3 + 3x^2l) \\ \psi_4(x) & = \frac{1}{l^3} (x^3l - x^2l^2) \end{aligned} \quad (28)$$

²⁹⁹ Employing the Galerkin method, the weak form of a
³⁰⁰ strong form equation given in Eq. (4) can be derived
³⁰¹ as [40]

³⁰²

$$\underbrace{\left[\int_0^l \psi^T \psi dx \right]}_{\mathbf{M}} \ddot{q}(t) + \underbrace{\left[\frac{\omega_n^2}{l^3} \int_0^l \frac{d^2 \psi}{dx^2}^T \frac{d^2 \psi}{dx^2} dx \right]}_{\mathbf{K}} q(t) + \underbrace{[k_1 \psi(0)]}_{\mathbf{L}} q(t)$$

³⁰³

$$+ \underbrace{\left[\epsilon c_1 \int_0^l \psi^T \psi dx + \epsilon c_2 \int_0^l \frac{d^2 \psi}{dx^2}^T \frac{d^2 \psi}{dx^2} dx \right]}_{\mathbf{C}} \dot{q}(t) + \underbrace{[\epsilon k_3 \psi(0)^3]}_{\mathbf{N}} q(t)^3 = 0 \quad (29)$$

³⁰⁴ The typical element mass matrix (\mathbf{M}), stiffness matrix ³²⁵
³⁰⁵ (\mathbf{K}), mass and stiffness proportional Rayleigh damping ³²⁶
³⁰⁶ matrix (\mathbf{C}) [57], and the linear and nonlinear spring stiff- ³²⁷
³⁰⁷ ness matrices (\mathbf{L} and \mathbf{N}) for a single unit have been de- ³²⁸
³⁰⁸rived as follows. ³²⁹

$$\mathbf{M} = \frac{1}{420} \begin{pmatrix} 156 & 22l & 54 & -13l \\ 22l & 4l^2 & 13l & -3l^2 \\ 54 & 13l & 156 & -22l \\ -13l & -3l^2 & -22l & 4l^2 \end{pmatrix}$$

$$\mathbf{K} = \omega_n^2 \begin{pmatrix} 12 & 6l & -12 & 6l \\ 6l & 4l^2 & -6l & 2l^2 \\ -12 & -6l & 12 & -6l \\ 6l & 2l^2 & -6l & 4l^2 \end{pmatrix}$$

$$\mathbf{C} = \frac{c_1}{420} \begin{pmatrix} 156 & 22l & 54 & -13l \\ 22l & 4l^2 & 13l & -3l^2 \\ 54 & 13l & 156 & -22l \\ -13l & -3l^2 & -22l & 4l^2 \end{pmatrix} + \frac{c_2}{l^3} \begin{pmatrix} 12 & 6l & -12 & 6l \\ 6l & 4l^2 & -6l & 2l^2 \\ -12 & -6l & 12 & -6l \\ 6l & 2l^2 & -6l & 4l^2 \end{pmatrix}$$

$$\mathbf{L} = \begin{pmatrix} k_1 & 0 & 0 & 0 \\ 0 & 0 & 0 & 0 \\ 0 & 0 & 0 & 0 \\ 0 & 0 & 0 & 0 \end{pmatrix}; \mathbf{N} = \begin{pmatrix} k_3 & 0 & 0 & 0 \\ 0 & 0 & 0 & 0 \\ 0 & 0 & 0 & 0 \\ 0 & 0 & 0 & 0 \end{pmatrix}$$

³²⁹ phenomena within both undamped and damped Euler-
³³⁰ Bernoulli beams supported by cubic nonlinearities, ex-
³³¹ ploring both hardening and softening nonlinear behav-
³³² iors. Additionally, it thoroughly examines the impact
³³³ of viscous damping and strain rate damping on damped
³³⁴ beams.

A. Numerical validation

³³⁵ The nonlinear dispersion relation can be derived us-
³³⁶ ing two approaches. The first is the free wave approach,
³³⁷ where the propagation constant (κ) is fixed by apply-
³³⁸ ing harmonic initial condition, and the corresponding
³³⁹ frequency (ω) is determined. Alternatively, the driven
³⁴⁰ wave approach fixes the frequency (ω) through harmonic
³⁴¹ boundary conditions, leading to the determination of
³⁴² the propagation constant. However, in dispersive me-
³⁴³ dia, the boundary complexity decreases the amplitude of
³⁴⁴ harmonic boundary conditions in the far field, impact-
³⁴⁵ ing the amplitude-dependent dispersion. Consequently,
³⁴⁶ for the nonlinear dispersion relation of infinite continuous
³⁴⁷ beams, the free wave approach is preferable for numerical
³⁴⁸ validation.

³⁴⁹ The MATLAB ODE45 function has been used to ob-
³⁵⁰tain the solution of the Eq. (33). For this, a very long
³⁵¹ beam has been simulated for a long time to get accu-
³⁵²rate fast Fourier transform (FFT) results but not so long
³⁵³ time that the boundary reflections affect the solution.
³⁵⁴ The FFT is calculated in both space and time to get
³⁵⁵wavenumber (κ) as well as frequency (ω). According to
³⁵⁶the free-wave approach, the frequency shift is obtained by
³⁵⁷fixing the wavenumber by imposing the initial condition
³⁵⁸as $w(x, 0) = A \cos(\kappa x)$, $w'(x, 0) = -A\kappa \sin(\kappa x)$.

³⁵⁹ For illustration purposes, the wave number $\kappa = 0.5$
³⁶⁰ and the amplitude $A = 1$ are applied in the initial condi-
³⁶¹tion to the beam shown in Fig. 2(a). Furthermore, the
³⁶²stiffness of the elastic springs is taken as $k_1 = 1$, $k_3 = -1$
³⁶³and $\epsilon = 1$ for the undamped system. In Fig. 2(b), the
³⁶⁴displacement profile of the center portion of the beam

³¹⁶ Further, the global matrices ($[]_g$) have been obtained and ³⁵⁷
³¹⁷ the global equation of motion can be written as follows. ³⁵⁸

$$\mathbf{M}_g \ddot{\mathbf{v}} + \mathbf{K}_g \mathbf{v} + \mathbf{L}_g \mathbf{v} + \epsilon (\mathbf{C}_g \dot{\mathbf{v}} + \mathbf{N}_g \mathbf{v}^3) = 0 \quad (33)$$

³¹⁸ where \mathbf{v} is the global displacement vector.

III. RESULTS AND DISCUSSION

³²¹ In this section, the proposed theory for nonlinear wave ³⁶⁶
³²² propagation has been validated with the numerical solu- ³⁶⁷
³²³tion. Further, this section discusses the wave dispersion ³⁶⁸

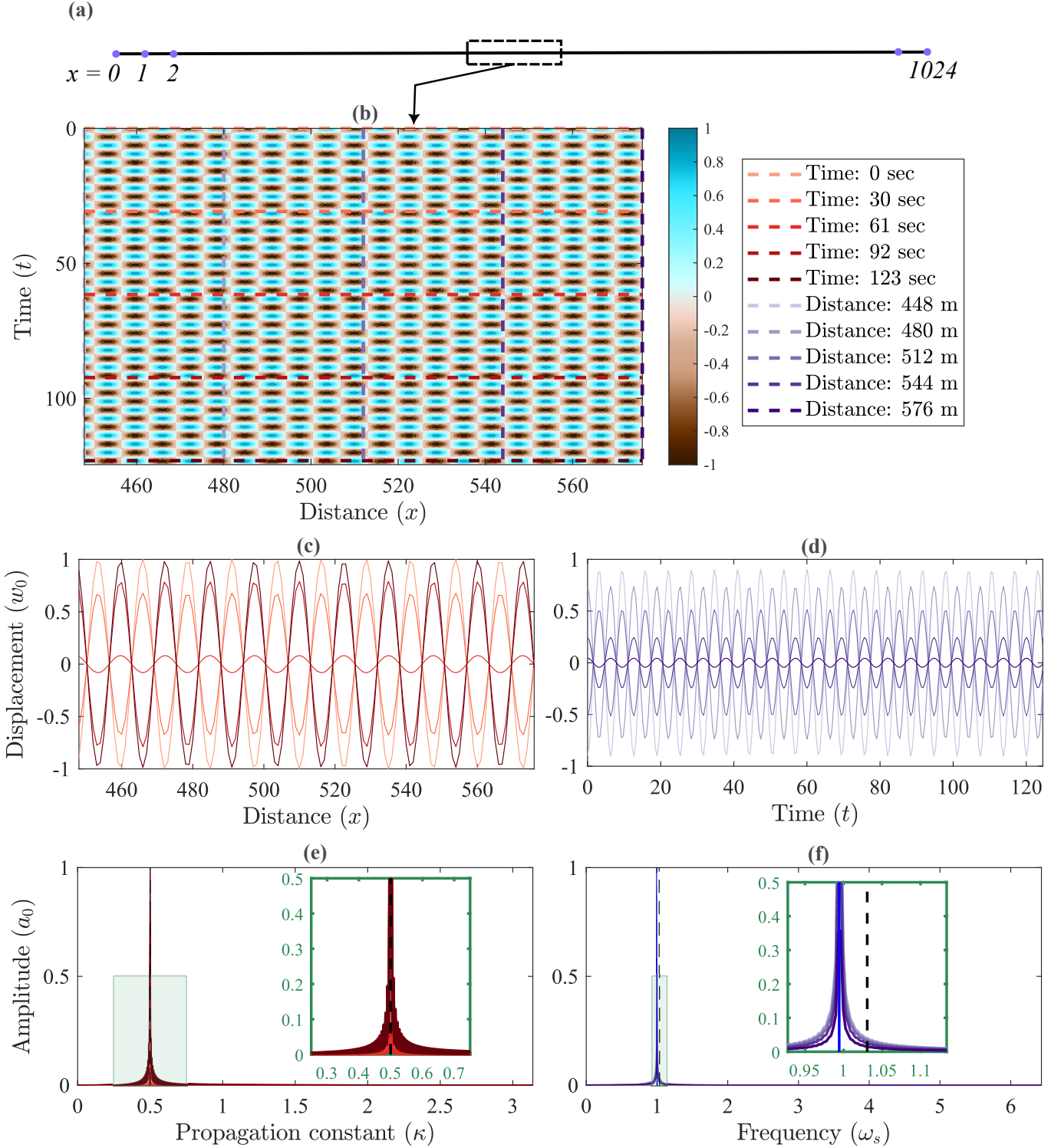


FIG. 2. (a) The long Euler Bernoulli beam with $c_1 = c_2 = 0, k_3 = -1, k_1 = 1, A = 1, \epsilon = 0.1$, (b) Displacement contour of the middle portion of the beam shown by the dashed box, (c) Displacement versus distance plot at different instances of time shown in horizontal dashed lines with orange shades in (b), (d) Displacement versus time plot at different locations shown in vertical dashed lines with violet shades in (b), (e) FFT plots corresponding to displacement profiles shown in (c), (f) FFT plots corresponding to time histories shown in (d).

with respect to space and time is demonstrated. Fur₃₇₁ different times as shown by the horizontal dashed line in
 ther, the beam displacement with respect to space at₃₇₂ Fig. 2(b) are plotted in Fig. 2(c), and its FFT plots

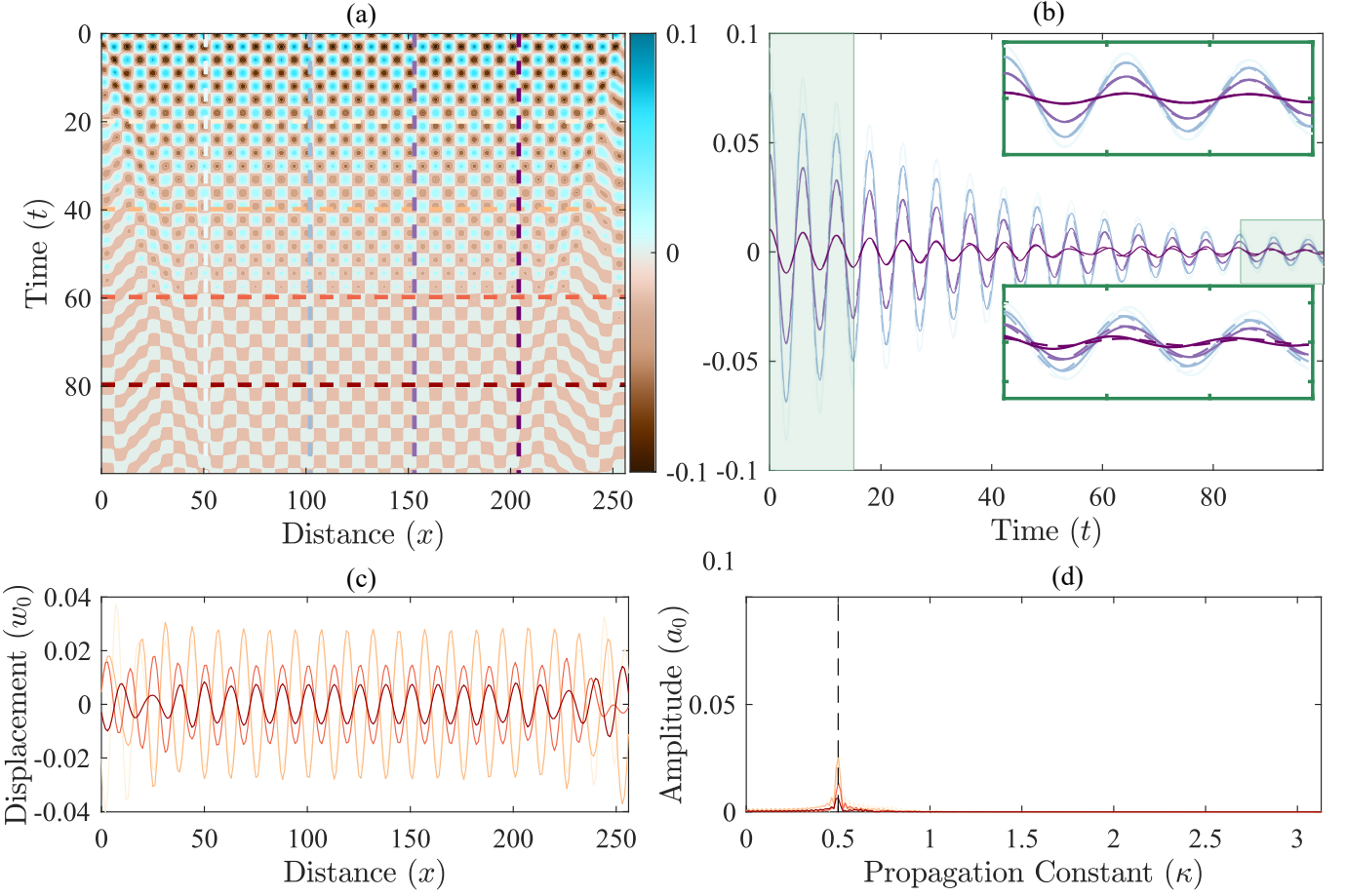


FIG. 3. (a) Displacement contour of the Euler Bernoulli beam with $c_1 = c_2 = 0.05, k_3 = 1, k_1 = 1, A = 0.1, \epsilon = 1$; (b) Displacement versus time plot at different locations shown in vertical dashed lines with violet shades in (a) where the solid lines depict numerical solution and the dashed lines depict analytical solution, moreover the magnified plots are shown inside to showcase the better validation in the initial time window and degraded validation in later time window; (c) Displacement versus distance plot at different instances of time shown in horizontal dashed lines with orange shades in (a); (d) FFT plots corresponding to displacement profiles shown in (c).

are plotted in Fig. 2(e) which shows peak amplitude at the wavenumber ($\kappa = 0.5$) applied in the initial condition. Furthermore, the beam displacement with respect to time at different spaces located by vertical dashed lines as shown in Fig. 2(b) are plotted in Fig. 2(d), and its FFT can be observed in Fig. 2(f). The peak amplitude frequency in Fig. 2(f) matches exactly with the analytically obtained nonlinear frequency shown with a solid blue line. As the nonlinearity is soft the frequency shift is negative which can be seen in the magnified plot in Fig. 2(f), where the frequency of the linear system is shown by a black dashed line. This validates the proposed theory of the free wave approach for an undamped system.

The damped system has been validated further in Fig. 3 with the following parameters: spring stiffness with hard nonlinearity as $k_1 = 1, k_3 = 1$, the damping factor $c_1 = c_2 = 1$ and $\epsilon = 1$. In addition, the initial condition is kept similar to the undamped case as the wave number $\kappa = 0.5$ and the amplitude $A = 1$. The displacement profile of the beam in space-time is illustrated in Fig.

3(a) which shows the decreases in amplitude as time progresses. However, the wavelength is constant as shown in Fig. 3(c) in which the displacement is plotted at different times shown by horizontal dashed lines in Fig. 3(a). Further, its FFT is plotted in Fig. 3(d), which shows the consistent wavenumber at different times. Furthermore, the time histories at different locations shown by vertical dashed lines in Fig. 3(b) are plotted in Fig. 3(b). The decrease in amplitude due to damping reduces the frequency shift with time, therefore instead of FFT of time histories for validation, the analytical displacement time histories are plotted with dashed lines to validate the proposed theory for the damped system. In magnified subplots of Fig. 3(b), the analytical and numerical solution matches exactly in the initial phase (Fig. 3(b1)) however, they deviate in long time as shown in Fig. 3(b2) as the analytical solution is valid till time inversely proportional to the scaling factor (ϵ) [16].

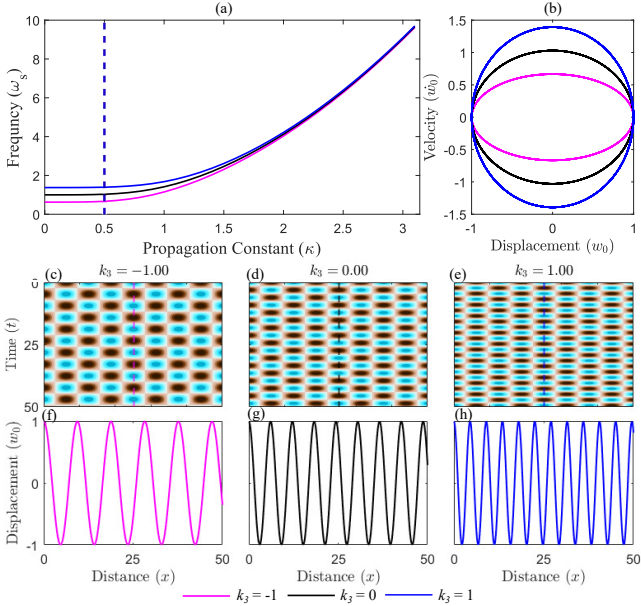


FIG. 4. (a) Dispersion relation plot for undamped system with $c_1 = c_2 = 0, k_1 = 1$ and nonlinear stiffness parameter $k_3 = -1, 0$ and 1 ; (b) Phase portrait for propagation constant $\kappa = 0.5$; (c) displacement profile for $\kappa = 0.5, k_3 = -1$; (d) displacement profile for $\kappa = 0.5, k_3 = 0$; (e) displacement profile for $\kappa = 0.5, k_3 = 1$; (f) Displacement time history at middle node of the beam with $\kappa = 0.5, k_3 = -1$; (g) Displacement time history at the middle node of the beam with $\kappa = 0.5, k_3 = 0$; (h) Displacement time history at the middle node of the beam with $\kappa = 0.5, k_3 = 1$.

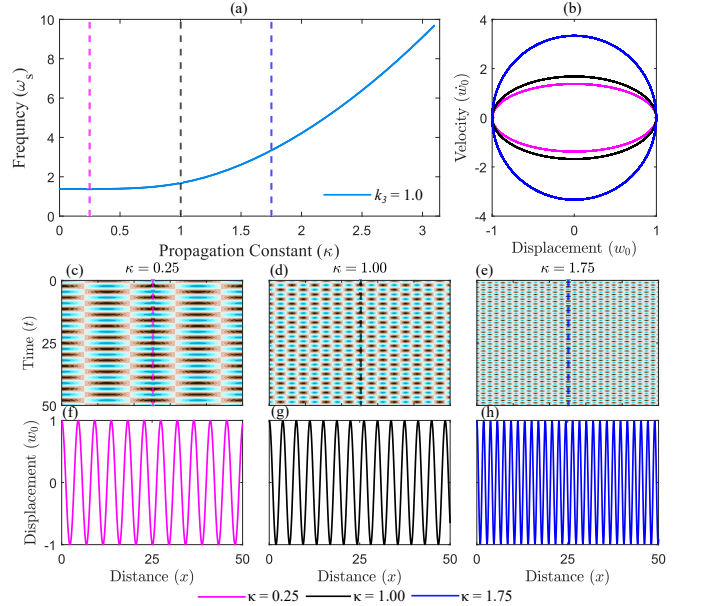


FIG. 5. (a) Dispersion relation plot for the undamped system with $c_1 = c_2 = 0, k_1 = 1, k_3 = 1$; (b) Phase portrait for propagation constant $\kappa = 0.25, 1.00$ and 1.75 ; (c) displacement profile for $\kappa = 0.25, k_3 = 1$; (d) displacement profile for $\kappa = 1.00, k_3 = 1$; (e) displacement profile for $\kappa = 1.75, k_3 = 1$; (f) Displacement time history at middle node of the beam with $\kappa = 0.25, k_3 = 1$; (g) Displacement time history at middle node of the beam with $\kappa = 1.00, k_3 = 10$; (h) Displacement time history at middle node of the beam with $\kappa = 1.75, k_3 = 1$.

Additionally, to analyze the impact of propagation constant, three different propagation constants: $\kappa = 0.25, 1$, and 2 have been considered, for a nonlinear system with hardening stiffness $k_3 = 1$, as depicted in the dispersion plot in Fig. 5(a). Furthermore, the displacement profile of free vibration is illustrated using contour plots in Fig. 5(c-e). The temporal response of the midpoint of the beam is shown in Fig. 5(f-h), accompanied by its corresponding phase portrait in Fig. 5(b). It is evident from these analyses that as the propagation constant increases, the corresponding frequency also increases, with the increment being minimal until propagation constant $\kappa = 1$.

C. Damped system

The effect of viscous damping and strain rate damping along with system nonlinearity on wave dispersion has been discussed in this section. The following three types of systems have been discussed.

1. Viscous damping $c_1 = 0.25$ and Strain rate damping $c_2 = 0$
2. Viscous damping $c_1 = 0$ and Strain rate damping $c_2 = 0.25$

411

B. Undamped system

This section presents an analysis of the dispersion relation of the nonlinear undamped system based on the proposed analytical plane wave solution. Initially, the influence of soft and hard nonlinearity on wave dispersion is investigated, as illustrated in Fig. 4, considering nonlinear spring stiffness values of $k_3 = -1, 0$, and 1 . An amplitude of $A = 1$ and a scaling parameter of $\epsilon = 1$ have been assumed. In Fig. 4(a), the dispersion plot is generated by varying the propagation constant (κ) from 0 to π to obtain the frequency ω_s using Eq. (25). As the frequency shift is inversely proportional to the frequency, it can be noticed that frequency shift is higher at low propagation constants and it diminishes at higher wavenumbers. Subsequently, in Fig. 4(c-e), we display the displacement contours for the free vibration of the beam for $\kappa = 0.5$. It is noteworthy that while the wave number remains consistent across all three figures, the temporal frequency increases as the nonlinear spring stiffness escalates. Similarly, in Fig. 4(f-h), we plot the response of the midpoint of the beam. Additionally, the corresponding phase portrait is depicted in Fig. 4(b), clearly illustrating the positive and negative shifts in frequency for the hardening and softening systems, respectively, from the linear dispersion.

436

437

438

439

440

441

442

443

444

445

446

447

448

449

450

451

452

453

454

455

456

457

458

459

460

461

462

463

464

465

466

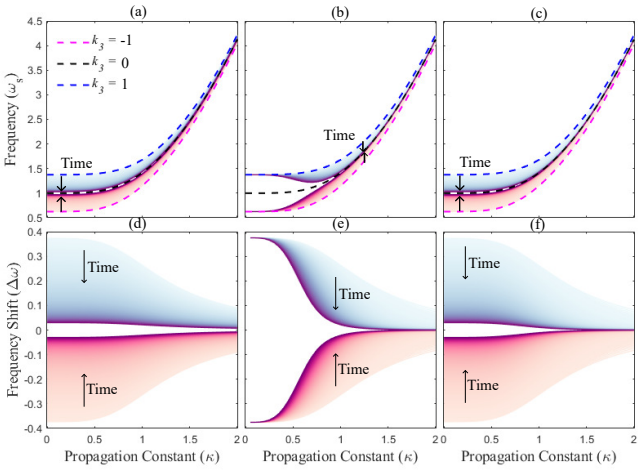


FIG. 6. Dispersion relation plots at different time instances are illustrated for hardening system with blue shades and softening system with shades of pink for (a) only viscous damping $c_1 = 0.25$ and $c_2 = 0$, (b) only strain rate damping $c_1 = 0$ and $c_2 = 0.25$ and (c) viscous damping and strain rate damping $c_1 = 0.25$ and $c_2 = 0.25$; Frequency shift versus propagation constant (κ) plots at different time instances are illustrated for hardening system with blue shades and softening system with shades of pink for (d) only viscous damping $c_1 = 0.25$ and $c_2 = 0$, (e) only strain rate damping $c_1 = 0$ and $c_2 = 0.25$ and (f) viscous damping and strain rate damping $c_1 = 0.25$ and $c_2 = 0.25$

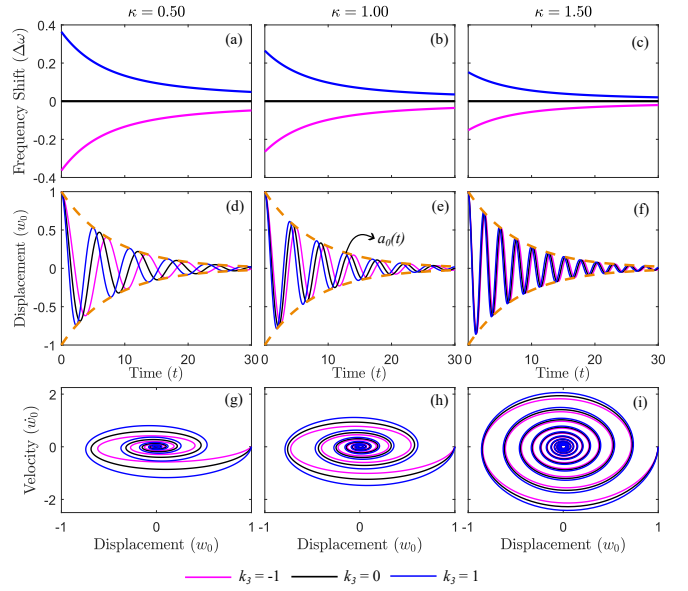


FIG. 7. Damped nonlinear system with only viscous damping $c_1 = 0.25$; $c_2 = 0$ and $k_1 = 1$. (a), (b) and (c) shows a frequency shift ($\Delta\omega$) versus time (t) propagation constant $\kappa = 0.50, 1.00$ and 1.50 respectively; (d), (e) and (f) show displacement (w_0) versus time (t) at the middle node of beam for propagation constant $\kappa = 0.50, 1.00$ and 1.50 respectively and yellow dashed line is for amplitude envelope; (g), (h) and (i) shows phase portraits for middle node of beam for propagation constant $\kappa = 0.50, 1.00$ and 1.50 respectively.

458 3. Viscous damping $c_1 = 0.25$ and Strain rate damping $c_2 = 0.25$

460 The dispersion relation plots of frequency (ω) versus 461 propagation constant (κ) are presented in Fig. 6(a, b, 462 and c) for the aforementioned configurations, represent- 463 ing only viscous damping, only strain rate damping, and 464 combined viscous and strain rate damping, respectively. 465 Considering the time-dependent nature of frequency shift 466 corresponding to propagation constants, the dispersion is 467 visualized at multiple time instances ranging from 0 to 468 100 seconds for both softening and hardening systems. 469 The evolution of these plots reveals a transition from un- 470 damped to linear system behavior over time. 498

471 Furthermore, the plots of frequency shift ($\Delta\omega$) ver- 472 sus propagation constant (κ) in Fig. 6(d-f) for all three 473 damping configurations highlight a decreasing trend in 474 frequency shift with increasing time. Notably, for sys- 475 tems with only strain rate damping (c_2), the damping 476 effect is proportional to κ^4 , resulting in a more rapid de- 477 cay for higher wavenumbers. Conversely, systems with 478 viscous damping (c_1) exhibit a damping effect indepen- 479 dent of wavenumber. In damped systems, nonlinear ef- 480 fects tend to diminish with decaying amplitudes. 508

481 First, we investigate the influence of viscous damping 509 on the behavior of a system under varying propagation 510 constants. Specifically, we focus on three distinct prop- 511 agation constants, namely $\kappa = 0.50, 1.00$, and 1.50 , ex- 512 amining the dynamics of frequency shift over time. This 513

analysis is presented through plots in Fig. 7 (a, b, and c), where differentiating characteristics of damping effects are delineated for hardening (magenta line), softening (blue line), and linear (black line) systems. Our findings reveal a convergence of frequency shifts to zero over time across all propagation constants, indicating consistent trends irrespective of the system's nonlinearity. Furthermore, the temporal evolution of displacement at the beam's middle node is depicted in Fig. 7 (d, e, and f) for $\kappa = 0.50, 1.00$, and 1.50 , respectively. In addition to these plots, the amplitude modulation, represented by the yellow dashed line, remains uniform across different propagation constants and types of nonlinearity. Additionally, phase portraits are presented in Fig. 7 (g, h, and i) for the same set of propagation constants. Notably, higher propagation constants correspond to higher velocities, indicative of increased frequencies. Moreover, the phase portraits elucidate distinct shifts from linear frequency: positive for hardening and negative for softening nonlinear systems, underscoring characteristic nonlinear behaviors. Additionally, we explore the impact of strain rate damping on systems characterized by diverse propagation constants. The damping factor corresponding to strain rate damping is proportional to κ^4 , so the amplitude modulation varies with the propagation constant. The temporal evolution of frequency shift is depicted in Fig. 8(a, b, and c) for propagation constants $\kappa = 0.5, 1.00$, and 1.50 , respectively. Notably, the rate

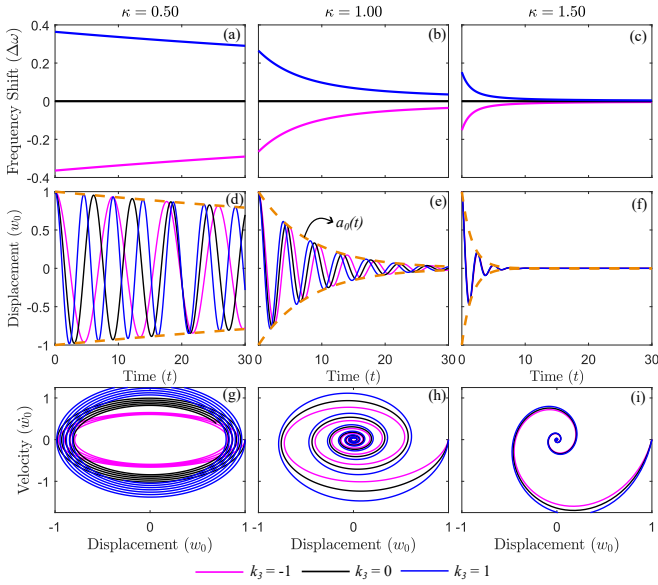


FIG. 8. Damped nonlinear system with only viscous damping $c_1 = 0; c_2 = 0.25$ and $k_1 = 1$. (a), (b) and (c) shows a frequency shift ($\Delta\omega$) versus time (t) propagation constant $\kappa = 0.50, 1.00$ and 1.50 respectively; (d), (e) and (f) show displacement (w_0) versus time (t) at the middle node of beam for propagation constant $\kappa = 0.50, 1.00$ and 1.50 respectively and the yellow dashed line is for amplitude envelope; (g), (h) and (i) shows phase portraits for the middle node of beam for propagation constant $\kappa = 0.50, 1.00$ and 1.50 respectively.

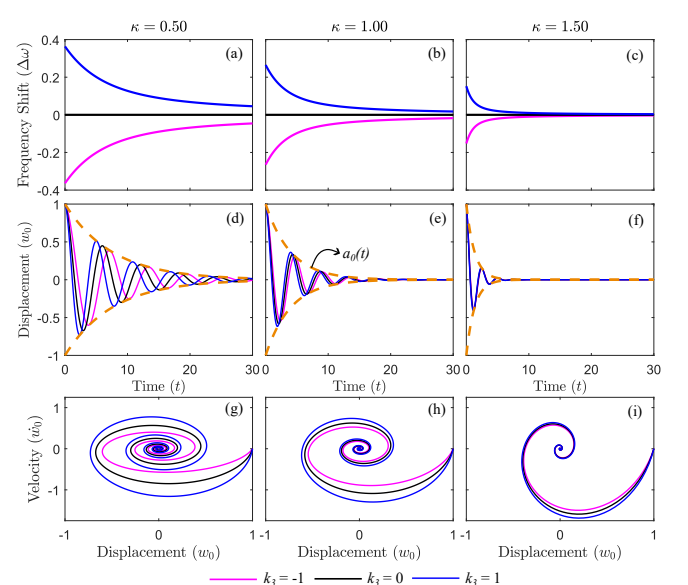


FIG. 9. Damped nonlinear system with only viscous and strain rate damping combine $c_1 = 0.25; c_2 = 0.25$ and $k_1 = 1$. (a), (b) and (c) shows a frequency shift ($\Delta\omega$) versus time (t) propagation constant $\kappa = 0.50, 1.00$ and 1.50 respectively; (d), (e) and (f) show displacement (w_0) versus time (t) at the middle node of beam for propagation constant $\kappa = 0.50, 1.00$ and 1.50 respectively and yellow dashed line is for amplitude envelope; (g), (h) and (i) shows phase portraits for middle node of beam for propagation constant $\kappa = 0.50, 1.00$ and 1.50 respectively.

of decrease in frequency shift varies significantly across different propagation constants, being notably slower for lower values of κ and more rapid for higher values. Upon examining the amplitude modulation for all three propagation constants in Fig. 8(d, e, and f), it becomes apparent that the decay progresses at a relatively slow pace when $\kappa = 0.50$, whereas it accelerates swiftly when $\kappa = 1.50$. Similarly, the phase portraits presented in Fig. 8(g, h, and i) for $\kappa = 0.5, 1.00$, and 1.50 reinforce these observations, providing further clarity on the relationship between propagation constants and damping effects.

Furthermore, we examine the combined effect of both types of damping, as illustrated in Fig. 9. The plots depicting frequency shift over time are presented in Fig. 9(a, b, and c) for propagation constants $\kappa = 0.5, 1.00$, and 1.50 , respectively. Notably, the frequency shift gradually diminishes over time, converging towards the frequency of a linear system as time progresses. Additionally, the amplitude modulation shown in Fig. 9(d, e, and f) elucidates the increase in decay rate with propagation constant. In the lower range of propagation constants, amplitude decay is primarily attributed to viscous damping, whereas in the higher range, it is predominantly due to strain rate damping. To gain a clearer understanding, phase portraits are depicted in Fig. 8(g, h, and i) for $\kappa = 0.5, 1.00$, and 1.50 , respectively, reinforcing these observations.

IV. SUMMARY AND CONCLUSION

In this paper, the analytical closed-form dispersion relation equation for a damped slender elastic beam periodically supported by cubic nonlinear springs has been derived. To derive the nonlinear dispersion relation, the method of multiple scales is employed after introducing a scaling parameter, ϵ , to account for slow time scales. Through this approach, the governing partial differential equation is expanded and solved iteratively, leading to expressions for complex amplitudes and frequency shifts. The amplitude modulation and frequency shift equations are derived as functions of damping coefficients and amplitude of the initial plane wave. The proposed theory for nonlinear wave propagation was validated numerically through finite element formulation. Numerical simulations were carried out using the MATLAB ODE45 function. The results of numerical and analytical solutions of the undamped and damped systems show consistency which affirms the validity of the developed analytical closed-form solutions.

An extensive investigation into wave dispersion in nonlinear undamped systems was carried out using an analytical plane wave solution. The key findings are as follows:

- For a given propagation constant, there will be an

amplitude-dependent shift in frequency. The positive shift is observed for hardening springs and negative for softening springs.

- Since the frequency shift is inversely proportional to the frequency of the corresponding linear system, nonlinearity has a greater impact at low propagation constants or low frequencies and it reduces with increasing propagation constants or frequencies.

Additionally, the study thoroughly investigates the effects of viscous damping and strain rate damping, both individually and in combination. Through the analysis of amplitude modulation and phase portraits, distinct behaviors were elucidated across systems with different propagation constants and damping effects. The key findings are summarized as follows:

- Over time, the amplitude-dependent frequency shift decreases and eventually reaches zero, regardless of propagation constants or damping type. Hence, the influence of nonlinearity diminishes over time in a damped system.
- Analysis of viscous damping revealed a consistent decay in frequency shifts over time across all propagation constants, while amplitude modulation remained uniform.
- The rate at which the amplitude decays in a system with strain rate damping is directly proportional to the fourth power of propagation constant. This leads to a relatively sluggish convergence of the frequency shift to zero at low propagation constants, but quite more rapid convergence at higher propagation constants.
- Furthermore, the combined effect of both types of damping illustrated a gradual convergence of frequency towards that of a linear system as time progressed. Amplitude decay was primarily attributed to viscous damping at lower propagation constants and strain rate damping at higher propagation constants.

This study has the following major contributions:

- A closed-form equation for amplitude-dependent dispersion relation has been derived for continuous systems, providing a valuable analytical tool for further research in this domain.
- Furthermore, the incorporation of damping effects into the analysis of nonlinear dispersion offers insights into emulating real-world behavior, enhancing the applicability and relevance of the findings.

ACKNOWLEDGEMENTS

Abhigna Bhatt and Arnab Banerjee acknowledge the Inspire faculty grant, grant number: DST/ INSPIRE/04/2018/000052, for partially supporting the research.

Appendix A: Multiple spatial scales approach

The nonlinear partial differential equation, as shown in Eq. (4), involves the independent variables x and t , which correspond to the spatial and temporal dimensions, respectively. By employing a multiscale method, additional scales are introduced to account for long spatial scales, defined as $X_1 = \epsilon x$, which augment the original spatial scale $X_0 = x$. Consequently, the spatial derivatives can be expressed as

$$\frac{\partial}{\partial x} = \frac{\partial}{\partial X_0} + \epsilon \frac{\partial}{\partial X_1} \quad (\text{A1})$$

Further, the solution can be obtained as

$$w(x, t, \epsilon) = \sum_{n=0}^1 \epsilon^n w_n(X_0, X_1, t) + O(\epsilon) \quad (\text{A2})$$

By substituting the solution given in Eq. (A2) into the partial differential equation given in Eq. (4) and employing the spatial derivatives provided in Eq. (A1), the governing partial differential equation can be expressed through the consolidation of terms with similar powers of ϵ as.

$$R_0 + R_1 \epsilon + O(\epsilon^2) = 0 \quad (\text{A3})$$

where

$$R_0 : \frac{\partial^4 w_0}{\partial X_0^4} + \frac{\partial^2 w_0}{\partial t^2} + k_1 w_0 = 0 \quad (\text{A4})$$

$$R_1 : \frac{\partial^4 w_1}{\partial X_0^4} + 4 \frac{\partial^4 w_0}{\partial X_1 \partial X_0^3} + \frac{\partial^2 w_1}{\partial t^2} + k_1 w_1 + c_1 \frac{\partial w_0}{\partial t} + c_2 \frac{\partial^5 w_0}{\partial t \partial X_0^4} + k_3 w_0^3 = 0 \quad (\text{A5})$$

The solutions w_0 , and w_1 can be obtained by solving equations $R_0 = 0$ and $R_1 = 0$ in progression.

In the case of flexural wave solution in infinite structure, the boundary complexities can be ignored and the plane wave solution can be assumed for the equation $R_0 = 0$.

$$w_0 = A(X_1) e^{i(\kappa X_0 - \omega t)} + \bar{A}(X_1) e^{-i(\kappa X_0 - \omega t)} \quad (\text{A6})$$

Substituting Eq. (A6) in Eq. (A4) the dispersion relation for the linear system can be derived as

$$\kappa^4 - \omega^2 + k_1 = 0 \quad (\text{A7})$$

652 Further, substituting Eq. (A6) in Eq. (A5), the following
653 equation can be obtained

$$\begin{aligned} 654 \quad & \frac{\partial^2 w_1}{\partial t^2} + \frac{\partial^4 w_1}{\partial X_0^4} + k_1 w_1 \\ 655 \quad & = \left(4i\kappa^3 \frac{\partial A}{\partial X_1} + ic_1\omega A + ic_2\kappa^4\omega A - 3k_3A^2\bar{A} \right) e^{i(\kappa X_0 - \omega t)} \\ 656 \quad & - k_3A^3e^{i(3\kappa X_0 - 3\omega t)} + cc \end{aligned} \quad (A8)$$

657 The particular solution of Eq. (A8) contains secular
658 terms which lead to nonuniform expansion in scaled
659 time. Since the linear operator $\left(\frac{\partial^2}{\partial t^2} + \frac{\partial^4}{\partial X_0^4} + k_1 \right)$ is self-
660 adjoint, as demonstrated in the appendix A, the solv-
661 ability condition for eliminating secular terms can be de-
662 rived. This condition is obtained by equating the forc-
663 ing terms responsible for generating the secular terms
664 to zero, which leads to the following partial differential
665 equation governing the amplitude A .

$$\begin{aligned} 666 \quad & 4i\kappa^3 \frac{\partial A}{\partial X_1} + ic_1\omega A + ic_2\kappa^4\omega A - 3k_3A^2\bar{A} = 0 \\ 667 \quad & i \frac{\partial A}{\partial X_1} = -iA \left(\frac{c_1 + c_2\kappa^4}{4\kappa^3} \right) \omega + \frac{3}{4\kappa^3} k_3A^2\bar{A} \end{aligned} \quad (A9)$$

668 The solution of A in polar form can be assumed as
669 $A = \frac{1}{2}a(X_1)e^{i\beta(X_1)}$, $\bar{A} = \frac{1}{2}a(X_1)e^{-i\beta(X_1)}$ and substitut-
670 ing them into Eq. A9 the following equations can be
671 obtained.

$$\begin{aligned} 672 \quad & i \frac{1}{2} \left(e^{i\beta} \frac{\partial a}{\partial X_1} + ie^{i\beta} a \frac{\partial \beta}{\partial X_1} \right) \\ 673 \quad & = -i \left(\frac{c_1 + c_2\kappa^4}{4\kappa^3} \right) \omega \frac{a}{2} e^{i\beta} + \frac{3}{4\kappa^3} k_3 e^{i\beta} \frac{a^3}{8} \end{aligned} \quad (A10)$$

674 Further separating the real and imaginary parts following
675 equations can be obtained.

$$\frac{\partial a}{\partial X_1} = - \left(\frac{c_1 + c_2\kappa^4}{4\kappa^3} \right) \omega a \quad (A11)$$

$$\frac{\partial \beta}{\partial X_1} = - \frac{3}{16\kappa^3} k_3 a^2 \quad (A12)$$

678 The amplitude modulation can be obtained by solving
679 Eq. (A11) as

$$a = a_0 e^{-\left(\frac{c_1 + c_2\kappa^4}{2\kappa^3} \right) \omega X_1} \quad (A13)$$

681 Further, the wave number shift can be obtained by sub-
682 stituting Eq. (A13) into Eq. (A12) as follows.

$$\begin{aligned} 683 \quad & \frac{\partial \beta}{\partial X_1} = - \frac{3}{16\kappa^3} k_3 a_0^2 e^{-\left(\frac{c_1 + c_2\kappa^4}{2\kappa^3} \right) \omega X_1} \\ 684 \quad & \beta = \frac{3}{8} \frac{k_3 a_0^2 \omega^{-1}}{(c_1 + c_2\kappa^4)} e^{-\left(\frac{c_1 + c_2\kappa^4}{2\kappa^3} \right) \omega X_1} + \beta_0 \end{aligned} \quad (A14)$$

Further, the initial condition has been assumed as at $X_1 = 0$, $\beta = 0$ and so, $\beta_0 = -\frac{3}{8} \frac{k_3 a_0^2 \omega^{-1}}{(c_1 + c_2\kappa^4)}$. The shift in frequency can be determined as

$$\begin{aligned} \beta &= \frac{3}{8} \frac{k_3 a_0^2 \omega^{-1}}{(c_1 + c_2\kappa^4)} e^{-\left(\frac{c_1 + c_2\kappa^4}{2\kappa^3} \right) \omega X_1} - \frac{3}{8} \frac{k_3 a_0^2 \omega^{-1}}{(c_1 + c_2\kappa^4)} \\ \beta &= -\frac{3}{8} \frac{k_3 \omega^{-1} a_0^2}{(c_1 + c_2\kappa^4)} \left(1 - e^{-\left(\frac{c_1 + c_2\kappa^4}{2\kappa^3} \right) \omega X_1} \right) \\ \beta &= -\frac{3}{8} \frac{k_3 \omega^{-1} a_0^2}{(c_1 + c_2\kappa^4)} \left(1 - e^{-\left(\frac{c_1 + c_2\kappa^4}{2\kappa^3} \right) \omega \epsilon x} \right) \end{aligned} \quad (A15)$$

Using the Eq. (A15), the shift in wavenumber can be determined. However, to obtain the frequency shift the concept of group velocity in amplitude modulation equation has been used. Further, from differentiating the Eq. (A7) with propagation constant κ the group velocity ($v_g = \frac{d\omega}{d\kappa}$) can be obtained as

$$\begin{aligned} 4\kappa^3 - 2\omega \frac{d\omega}{d\kappa} &= 0 \\ v_g &= \frac{d\omega}{d\kappa} = \frac{2\kappa^3}{\omega} \end{aligned} \quad (A16)$$

Now, by substituting Eq. (A16) into Eq. (A13) and Eq. (A15), and incorporating $v_g = x/t$ the following equation can be determined

$$a = a_0 e^{-(c_1 + c_2\kappa^4)\epsilon t} \quad (A17)$$

$$\beta = -\frac{3}{8} \frac{k_3 \omega^{-1} a_0^2}{(c_1 + c_2\kappa^4)} \left(1 - e^{-(c_1 + c_2\kappa^4)\epsilon t} \right) \quad (A18)$$

Equations A17 and A18 match exactly with the solutions obtained using temporal multiscales in Eqs. 19 and 21. Thus, it can concluded that both temporal and spatial methods of multiple scales can be used to determine nonlinear frequency shifts.

Appendix B: Proof of self ad-joint operator

To prove the left-hand side of Eq. (14) $\left(\frac{\partial^2}{\partial T_0^2} + \frac{\partial^4}{\partial x^4} + k_1 \right)$ self adjoined, first the variable separation method has been used to get two separate ordinary differential equations (ODE) as follows. Let, the solution $w(x, T_0) = f(x)g(T_0)$

$$\begin{aligned} \left(\frac{\partial^2}{\partial T_0^2} + \frac{\partial^4}{\partial x^4} + k_1 \right) w(x, T_0) &= 0 \\ \left(\frac{\partial^2}{\partial T_0^2} + \frac{\partial^4}{\partial x^4} + k_1 \right) f(x)g(T_0) &= 0 \\ f(x) \frac{d^2 g(T_0)}{dT_0^2} + G(T_0) \frac{d^4 f(x)}{dx^4} + k_1 f(x)g(T_0) &= 0 \end{aligned} \quad (B1)$$

718 dividing whole Eq. (B1) with $f(x)g(T_0)$ as

$$\frac{1}{g(T_0)} \frac{d^2g(T_0)}{dT_0^2} + \frac{1}{f(x)} \frac{d^4f(x)}{dx^4} + k_1 = 0 \quad (B2)$$

720 Further,

$$\frac{1}{g(T_0)} \frac{d^2g(T_0)}{dT_0^2} = -\frac{1}{f(x)} \frac{d^4f(x)}{dx^4} - k_1 = \lambda \quad (B3)^{734}$$

722 following this two separate ODEs can be written as

$$\frac{d^2g(T_0)}{dT_0^2} - \lambda g(T_0) = 0 \quad (B4)^{736}$$

$$\frac{d^4f(x)}{dx^4} + (k_1 + \lambda) f(x) = 0 \quad (B5)$$

725 The eigenvalue problem to solve is Eq. (B5) and the
726 Linear operator in is $(L = \frac{d^4}{dx^4})$. Operator L can be
727 called self ad-join if inner products $\langle Lu, v \rangle = \langle u, Lv \rangle$.

$$\begin{aligned} \langle Lu, v \rangle &= \int_a^b \left(\frac{d^4u(x)}{dx^4} \right) v(x) dx \\ &= \left[\frac{d^3u(x)}{dx^3} v(x) \right]_a^b - \int_a^b \frac{d^3u(x)}{dx^3} \frac{dv(x)}{dx} dx \quad (B6) \\ &= \left[\frac{d^3u(x)}{dx^3} v(x) \right]_a^b + \left[\frac{d^2u(x)}{dx^2} \frac{dv(x)}{dx} \right]_a^b \\ &\quad - \int_a^b \frac{d^2u(x)}{dx^2} \frac{d^2v(x)}{dx^2} dx \end{aligned} \quad (B7)^{744}$$

732 Further,

$$\langle u, Lv \rangle = \int_a^b u(x) \left(\frac{d^4v(x)}{dx^4} \right) dx \quad (B8)$$

$$= \left[\frac{d^3v(x)}{dx^3} u(x) \right]_a^b - \int_a^b \frac{d^3v(x)}{dx^3} \frac{du(x)}{dx} dx \quad (B9)$$

$$\begin{aligned} &= \left[\frac{d^3v(x)}{dx^3} u(x) \right]_a^b + \left[\frac{d^2v(x)}{dx^2} \frac{du(x)}{dx} \right]_a^b \\ &\quad - \int_a^b \frac{d^2v(x)}{dx^2} \frac{d^2u(x)}{dx^2} dx \end{aligned} \quad (B10)$$

737 After applying appropriate boundary conditions the Eq.
738 (B7) and Eq. (B10) can be proved to be the same. For
739 brevity in the case of the simply supported beam, the
740 boundary conditions $u(a) = 0, v(a) = 0, u(b) = 0$, and
741 $v(b) = 0$ can be substituted in the Eq. (B7) and Eq.
742 (B10). The inner product is:

$$\langle Lu, v \rangle = \langle u, Lv \rangle = - \int_a^b \frac{d^2u(x)}{dx^2} \frac{d^2v(x)}{dx^2} dx \quad (B11)$$

743 Hence, It can be said that the operator
744 $\left(\frac{\partial^2}{\partial T_0^2} + \frac{\partial^4}{\partial x^4} + k_1 \right)$ is self adjoined.

- [1] Sun, H., Zhang, S. & Shui, X. A tunable acoustic diode
771 made by a metal plate with periodical structure. *Applied Physics Letters*. **100** (2012)
772
- [2] Zhou, D., Ma, J., Sun, K., Gonella, S. & Mao, X. Switch-
774 able phonon diodes using nonlinear topological Maxwell
775 lattices. *Physical Review B*. **101**, 104106 (2020)
776
- [3] Li, F., Anzel, P., Yang, J., Kevrekidis, P. & Daraio, C.
777 Granular acoustic switches and logic elements. *Nature Communications*. **5**, 5311 (2014)
778
- [4] Jensen, J. Phononic band gaps and vibrations in one-
780 and two-dimensional mass-spring structures. *Journal Of Sound And Vibration*. **266**, 1053-1078 (2003)
781
- [5] Narisetti, R., Leamy, M. & Ruzzene, M. A perturba-
783 tion approach for predicting wave propagation in one-
784 dimensional nonlinear periodic structures. *Journal Of Vi-
785 bration And Acoustics*. **132**, 31001 (2010)
786
- [6] Xu, X., Barnhart, M., Fang, X., Wen, J., Chen, Y. &
787 Huang, G. A nonlinear dissipative elastic metamaterial
788 for broadband wave mitigation. *International Journal Of
789 Mechanical Sciences*. **164** pp. 105159 (2019)
790
- [7] Gong, C., Fang, X. & Cheng, L. Band degeneration and
791 evolution in nonlinear triatomic metamaterials. *Nonlinear Dynamics*. **111**, 97-112 (2023)
792
- [8] Campana, M., Ouisse, M., Sadoulet-Reboul, E., Ruzzene,
793 M., Neild, S. & Scarpa, F. Impact of non-linear res-

794 onators in periodic structures using a perturbation ap-
795 proach. *Mechanical Systems And Signal Processing*. **135**
796 pp. 106408 (2020)

- [9] Wu, K., Hu, H. & Wang, L. Nonlinear elastic waves
797 in a chain type of metastructure: theoretical analysis
798 and parametric optimization. *Nonlinear Dynamics*. **111**,
799 11729-11751 (2023)
- [10] Silva, P., Leamy, M., Geers, M. & Kouznetsova, V.
800 Emergent subharmonic band gaps in nonlinear locally
801 resonant metamaterials induced by autoparametric reso-
802 nance. *Physical Review E*. **99**, 063003 (2019)
- [11] Sepehri, S., Mashhadi, M. & Fakhrabadi, M. Nonlinear
803 nonlocal phononic crystals with roton-like behavior. *Non-
804 linear Dynamics*. **111**, 8591-8610 (2023)
- [12] Bae, M. & Oh, J. Amplitude-induced bandgap: New type
805 of bandgap for nonlinear elastic metamaterials. *Journal
806 Of The Mechanics And Physics Of Solids*. **139** pp. 103930
807 (2020)
- [13] Jiao, W. & Gonella, S. Doubly nonlinear waveguides with
808 self-switching functionality selection capabilities. *Physi-
809 cal Review E*. **99**, 042206 (2019)
- [14] Fang, X., Wen, J., Yu, D. & Yin, J. Bridging-coupling
810 band gaps in nonlinear acoustic metamaterials. *Physical
811 Review Applied*. **10**, 054049 (2018)

- [15] Nayfeh, A. & Mook, D. Nonlinear oscillations. (John Wiley & Sons,2008) 859
860
- [16] Nayfeh, A. Perturbation methods. (John Wiley & Sons,2008) 861
862
- [17] Marathe, A. & Chatterjee, A. Wave attenuation in non-linear periodic structures using harmonic balance and multiple scales. *Journal Of Sound And Vibration.* **289**, 863
864 871-888 (2006) 866
- [18] Sepehri, S., Mashhadi, M. & Fakhrabadi, M. Wave propagation in fractionally damped nonlinear phononic crystals. *Nonlinear Dynamics.* **110**, 1683-1708 (2022) 867
868 869
- [19] Sepehri, S., Mashhadi, M. & Fakhrabadi, M. Wave propagation in nonlinear monoatomic chains with linear and quadratic damping. *Nonlinear Dynamics.* pp. 1-22 (2022) 872
- [20] Liu, M. & Zhou, F. Spectro-spatial analysis of elastic wave propagation in nonlinear elastic metamaterial systems with damping. *Chaos: An Interdisciplinary Journal Of Nonlinear Science.* **32** (2022) 873
874 875
- [21] Xia, Y., Ruzzene, M. & Erturk, A. Bistable attachments for wideband nonlinear vibration attenuation in a meta-material beam. *Nonlinear Dynamics.* **102** pp. 1285-1296 (2020) 877
878 879
- [22] Kurt, M., Eriten, M., McFarland, D., Bergman, L. & Vakakis, A. Strongly nonlinear beats in the dynamics of an elastic system with a strong local stiffness nonlinearity: Analysis and identification. *Journal Of Sound And Vibration.* **333**, 2054-2072 (2014) 880
881 882
- [23] Herrera, C., McFarland, D., Bergman, L. & Vakakis, A. Methodology for nonlinear quantification of a flexible beam with a local, strong nonlinearity. *Journal Of Sound And Vibration.* **388** pp. 298-314 (2017) 883
884 885
- [24] Zhao, B., Thomsen, H., Pu, X., Fang, S., Lai, Z., Van Damme, B., Bergamini, A., Chatzi, E. & Colombi, A. A nonlinear damped metamaterial: Wideband attenuation with nonlinear bandgap and modal dissipation. *Mechanical Systems And Signal Processing.* **208** pp. 111079 (2024) 889
890 891
- [25] Casalotti, A., El-Borgi, S. & Lacarbonara, W. Metamaterial beam with embedded nonlinear vibration absorbers. *International Journal Of Non-Linear Mechanics.* **98** pp. 32-42 (2018) 892
893 894
- [26] Askari, H. & Esmailzadeh, E. Chaotic and periodic vibration of a carbon nanotube supported by nonlinear foundation. *14th IEEE International Conference On Nanotechnology.* pp. 632-635 (2014) 895
896 900
- [27] Norouzi, H. & Younesian, D. Chaotic vibrations of beams on nonlinear elastic foundations subjected to reciprocating loads. *Mechanics Research Communications.* **69** pp. 121-128 (2015) 904
905 906
- [28] Zang, J., Cao, R. & Zhang, Y. Steady-state response of a viscoelastic beam with asymmetric elastic supports coupled to a lever-type nonlinear energy sink. *Nonlinear Dynamics.* **105** pp. 1327-1341 (2021) 908
909 911
- [29] Khajehtourian, R. & I., H. Dispersion characteristics of a nonlinear elastic metamaterial. *AIP Advances.* **4** pp. 124308 (2014) 912
913 914
- [30] Manktelow, K., Leamy, M. & Ruzzene, M. Comparison of asymptotic and transfer matrix approaches for evaluating intensity-dependent dispersion in nonlinear photonic and phononic crystals. *Wave Motion.* **50**, 494-508 (2013) 915
916 918
- [31] Wang, K., Zhou, J., Xu, D. & Ouyang, H. Lower band gaps of longitudinal wave in a one-dimensional periodic rod by exploiting geometrical nonlinearity. *Mechanical Systems And Signal Processing.* **124** pp. 664-678 (2019) 919
920 921
- [32] Zhou, J., Dou, L., Wang, K., Xu, D. & Ouyang, H. A nonlinear resonator with inertial amplification for very low-frequency flexural wave attenuations in beams. *Nonlinear Dynamics.* **96** pp. 647-665 (2019)
- [33] Shen, Y. & Lacarbonara, W. Nonlinear dispersion properties of metamaterial beams hosting nonlinear resonators and stop band optimization. *Mechanical Systems And Signal Processing.* **187** pp. 109920 (2023)
- [34] Fronk, M., Fang, L., Packo, P. & Leamy, M. Elastic wave propagation in weakly nonlinear media and metamaterials: a review of recent developments. *Nonlinear Dynamics.* **111**, 10709-10741 (2023)
- [35] Chen, Z., Wang, G., Zhou, W. & Lim, C. Elastic foundation induced wide bandgaps for actively-tuned topologically protected wave propagation in phononic crystal beams. *International Journal Of Mechanical Sciences.* **194** pp. 106215 (2021)
- [36] Bae, M. & Oh, J. Nonlinear elastic metamaterial for tunable bandgap at quasi-static frequency. *Mechanical Systems And Signal Processing.* **170** pp. 108832 (2022)
- [37] Bera, K. & Banerjee, A. A consistent dynamic stiffness matrix for flutter analysis of bridge decks. *Computers & Structures.* **286** pp. 107107 (2023)
- [38] Burlon, A. & Failla, G. On the band gap formation in locally-resonant metamaterial thin-walled beams. *European Journal Of Mechanics-A/Solids.* **97** pp. 104798 (2023)
- [39] Cheng, X., Bergman, L., McFarland, D., Tan, C., Vakakis, A. & Lu, H. Co-existing complexity-induced traveling wave transmission and vibration localization in Euler-Bernoulli beams. *Journal Of Sound And Vibration.* **458** pp. 22-43 (2019)
- [40] Bathe, K. Finite element procedures. (Klaus-Jurgen Bathe,2006)
- [41] Fronk, M. & Leamy, M. Higher-order dispersion, stability, and waveform invariance in nonlinear monoatomic and diatomic systems. *Journal Of Vibration And Acoustics.* **139**, 051003 (2017)
- [42] Bonanomi, L., Theocharis, G. & Daraio, C. Wave propagation in granular chains with local resonances. *Physical Review E.* **91**, 033208 (2015)
- [43] Deng, B., Tournat, V. & Bertoldi, K. Effect of predeformation on the propagation of vector solitons in flexible mechanical metamaterials. *Physical Review E.* **98**, 053001 (2018)
- [44] Sánchez-Morcillo, V., Pérez-Arjona, I., Romero-García, V., Tournat, V. & Gusev, V. Second-harmonic generation for dispersive elastic waves in a discrete granular chain. *Physical Review E.* **88**, 043203 (2013)
- [45] Wallen, S. & Haberman, M. Nonreciprocal wave phenomena in spring-mass chains with effective stiffness modulation induced by geometric nonlinearity. *Physical Review E.* **99**, 013001 (2019)
- [46] Li, Q., Di Gialleonardo, E. & Corradi, R. Equivalent Models of an Infinite Track for Frequency and Time Domain Analyses. *Journal Of Vibration Engineering & Technologies.* pp. 1-23 (2024)
- [47] Nielsen, J. & Oscarsson, J. Simulation of dynamic train-track interaction with state-dependent track properties. *Journal Of Sound And Vibration.* **275**, 515-532 (2004)
- [48] Koroma, S., Hussein, M. & Owen, J. Vibration of a beam on continuous elastic foundation with nonhomogeneous stiffness and damping under a harmonically excited mass.

- 923 *Journal Of Sound And Vibration.* **333**, 2571-2587 (2014)⁹⁴⁷
- 924 [49] Hedayati, R. & Sadighi, M. A micromechanical approach⁹⁴⁸
925 to numerical modeling of yielding of open-cell porous⁹⁴⁹
926 structures under compressive loads. *Journal Of Theoret-950*
927 *ical And Applied Mechanics.* **54**, 769-781 (2016)⁹⁵¹
- 928 [50] Sadeghnejad, S., Taraz Jamshidi, Y., Mirzaeifar, R. &⁹⁵²
929 Sadighi, M. Modeling, characterization and parametric⁹⁵³
930 identification of low velocity impact behavior of time-⁹⁵⁴
931 dependent hyper-viscoelastic sandwich panels. *Proceed-955*
932 *ings Of The Institution Of Mechanical Engineers, Parts956*
933 *L: Journal Of Materials: Design And Applications.* **233**,⁹⁵⁷
934 622-636 (2019)⁹⁵⁸
- 935 [51] Zhang, X., Qiu, Y. & Griffin, M. Transmission of verti-⁹⁵⁹
936 cal vibration through a seat: Effect of thickness of foam⁹⁶⁰
937 cushions at the seat pan and the backrest. *International961*
938 *Journal Of Industrial Ergonomics.* **48** pp. 36-45 (2015)⁹⁶²
- 939 [52] Gibson, L., Ashby, M. & Harley, B. Cellular materials in⁹⁶³
940 nature and medicine. (Cambridge University Press,2010)⁹⁶⁴
- 941 [53] Ashby, M. Metal Foams: a design guide. (Butterworth-⁹⁶⁵
942 Heinemann College,2000)⁹⁶⁶
- 943 [54] Ghazwani, M., Alnujaie, A., Youzera, H., Meftah, S. &⁹⁶⁷
944 Tounsi, A. Nonlinear damping and forced vibration in-⁹⁶⁸
945 vestigation of three-layered viscoelastic sandwich beams⁹⁶⁹
946 on nonlinear elastic foundation with interlaminar contin-
- uous shear stress Zig-Zag theories. *Acta Mechanica.* **235**,
3557-3571 (2024)
- [55] Zamani, H., Nourazar, S. & Aghdam, M. Large-
amplitude vibration and buckling analysis of foam beams
on nonlinear elastic foundations. *Mechanics Of Time-
Dependent Materials.* **28**, 363-380 (2024)
- [56] Sun, Y., Han, Q., Jiang, T. & Li, C. Coupled bandgap
properties and wave attenuation in the piezoelectric
metamaterial beam on periodic elastic foundation. *Ap-
plied Mathematical Modelling.* **125** pp. 293-310 (2024)
- [57] Chopra, A. Dynamics of structures. (Pearson Education
India,2007)
- [58] Zhou, D., Rocklin, D., Leamy, M. & Yao, Y. Topological
invariant and anomalous edge modes of strongly nonlin-
ear systems. *Nature Communications.* **13**, 3379 (2022)
- [59] Ma, F., Tang, Z., Shi, X., Wu, Y., Yang, J., Zhou, D.,
Yao, Y. & Li, F. Nonlinear topological mechanics in el-
liptically geared isostatic metamaterials. *Physical Review
Letters.* **131**, 046101 (2023)
- [60] Banerjee, A. & Bera, K. Wave propagation in mass-in-
mass Duffing type non-linear metamaterial implementing
Jacobi's elliptic balance method. *International Journal
Of Non-Linear Mechanics.* **157** pp. 104549 (2023)